Nanoscale

PAPER

View Article Online
View Journal | View Issue

Cite this: *Nanoscale*, 2023, **15**, 10423

ALD/MLD coating of patterned vertically aligned carbon nanotube micropillars with Fe-NH_2TP hybrids†

R. M. Silva, *[a] J. Rocha *[b] and R. F. Silva [a]

The creation of nanoscale organic–inorganic hybrid coatings with uniform architecture and high surface area, while maintaining their structural and morphological integrity, remains a significant challenge in the field. In this study, we present a novel solution, by utilizing Atomic/Molecular Layer Deposition (ALD/MLD) to coat patterned vertically aligned carbon nanotube micropillars with a conformal amorphous layer of Fe-NH_2TP, which is a trivalent iron complex complexed with 2-amino terephthalate. The effectiveness of the coating is verified through multiple analytical techniques, including high-resolution transmission electron microscopy, scanning transmission electron microscopy, grazing incidence X-ray diffraction, and Fourier transform infrared spectroscopy. The Fe-NH_2TP hybrid film exhibits hydrophobic properties, as confirmed by water contact angle measurements. Our findings contribute to advancing the understanding of how to grow high-quality one-dimensional materials using ALD/MLD and hold promise for future research in this area.

Received 7th April 2023,
Accepted 7th June 2023

DOI: 10.1039/d3nr01610b

rsc.li/nanoscale

1. Introduction

The versatility of Atomic/Molecular Layer Deposition (ALD/MLD) has made it a popular choice for producing high-quality thin films of both amorphous and crystalline inorganic–organic hybrid materials. Its widespread recognition has resulted in a broad range of applications and integration into functional devices.[1] In addition to film growth, ALD is now being utilized for post-functionalization and manipulation of the defect and pore size distribution in powdered Metal Organic Frameworks (MOFs).[2] This has expanded the potential of ALD beyond its traditional use in creating high-k-dielectric materials, such as metal oxides, for microelectronics.[3]

Iron-bearing carboxylate Metal Organic Frameworks (MOFs) have garnered significant attention due to their unique structures and exceptional properties, making them suitable for a wide range of applications.[4,5] These MOFs are constructed from Fe, serving as an inorganic node, and the organic ligand terephthalic acid (TPA), such as MIL 101(Fe) and its amine-functionalized form NH_2-MIL-101(Fe).[6] While these materials are often synthesized as powders, there have been attempts to prepare them as thin films. The goal of reducing or eliminating the use of solvents in MOF synthesis is an active area of research.[7,8] Furthermore, it remains challenging to form thin films of these materials on high aspect ratio nanostructures using solution-based methods, while maintaining accurate control over film thickness and composition, which are critical parameters for device applications.

Here, we present the fabrication of a novel one-dimensional (1D) heterostructure that features a carbon nanotube core, a titanium oxide shell prepared by Atomic/Molecular Layer Deposition (ALD), and a functional organic–inorganic layer of trivalent iron complexed with 2-amino terephthalate (Fe-NH_2TP) coated by ALD/MLD. The titanium oxide layer serves as an adhesion layer, connecting the substrate carbon nanotubes to the functional layer, a common practice in nanofabrication.[9] Previous research by Stassen *et al.* has utilized titanium oxide as an adhesion layer in coating high aspect ratio silicon pillars with chemical vapor deposition of zeolitic imidazolate framework thin films.[10] Due to the ALD self-limiting nature, high quality, uniform, and conformal films may be deposited even on one-dimension to three-dimensional geometries, such as carbon nanotubes, nanowires, polymers, making this a robust technique to produce various multifunctional heterostructures.[11,12] MLD is, essentially, the organic counterpart of ALD, sharing the same intrinsic characteristics.[13] There

[a]*CICECO – Aveiro Institute of Materials, Department of Materials and Ceramic Engineering, University of Aveiro, 3810-193 Aveiro, Portugal. E-mail: rmsilva@ua.pt*
[b]*CICECO – Aveiro Institute of Materials, Department of Chemistry, University of Aveiro, 3810-193 Aveiro, Portugal. E-mail: rocha@ua.pt*

†Electronic supplementary information (ESI) available: Materials, XRR and GIXRD patterns, SEM image, 3D rendered AFM images, ATR-FTIR spectra, powder XRD pattern, Raman spectrum, STEM and EDX elemental mapping images, optical photograph of a film on Si/SiO_2 and vertically aligned carbon nanotube micropillars substrates. See DOI: https://doi.org/10.1039/d3nr01610b

is much room for research into the ALD/MLD growth conditions of TPA-based organic–inorganic hybrids as this aromatic dicarboxylic acid is a prevalent MLD organic ligand due to its rigid structure and high reactivity. The ALD/MLD process reported here is based on $Fe(thd)_3$, where thd = tris(2,2,6,6-tetramethyl-3,5-heptanedionate), and NH_2TPA reacted at a low deposition temperature, 170 °C. $Fe(thd)_3$ is a β-diketonate complex and this type of molecules exhibit low reactivity with water molecules and, thus, the processes usually require ozone as the oxygen source and a high deposition temperature.[14] To the best of our knowledge, the application of Atomic/Molecular Layer Deposition (ALD/MLD) technique to coat high aspect ratio substrates, such as periodic patterned vertically aligned carbon nanotube micropillars, with inorganic–organic hybrid thin films has not been reported previously. Carbon nanotubes are a promising support for these hybrid materials due to their superior mechanical, thermal, and electrical properties, combined with low density and high surface area. In order to harness these characteristics for new devices, it is essential to control the processing of vertically aligned carbon nanotubes into desired geometric patterns and architectures.[15] The proposed core–shell–shell heterostructure fabrication process is depicted schematically in Fig. 1.

2. Experimental section

2.1. Periodic carbon nanotube micropillars

Following Fig. 1a, the vertically aligned carbon nanotube micropillars were produced by thermal chemical vapor deposition using a patterned Ni catalyst (shadow masking) thin film on Si/SiO_2 substrate, from a gas mixture of $C_2H_2/H_2/Ar$ at 650 °C. The growth period was 15 min at atmospheric pressure. After growth, the samples were cooled down to room temperature below 100 °C, according to the thermal chemical vapor deposition steps summarized in Fig. S1.† In this growth process, a continuous Ni thin film undergoes catalyst nano-sized particle formation, which serves as the nucleation site for the subsequent growth of nanotubes (ref. 16). The shadow masking technique consisted of a circular hole array metallic mask with 500 μm diameter holes and a constant interspacing distance of 400 μm. Ni thin film was deposited on DC magnetron sputtering (PVD) using an Ar plasma (≈3.2×10^{-4} torr, room temperature) and a 10 minutes deposition time (12 nm thick thin film). For practical reasons, Ni catalyst was chosen over Fe catalyst to prevent any confusion in the interpretation of elemental analysis, as Fe is already a component of the hybrid thin films as an inorganic component. Prior to the Fe-NH_2TP deposition (Fig. 1b), the carbon nanotube micropillars were coated with titanium oxide by ALD on a tubular custom-made reactor at 100 °C using TTIP and de-ionized H_2O as the metal and oxygen precursors, respectively. The stainless-steel cylinder containing the TTIP precursor was heated at 80° C for optimal vapor pressure without decomposition, while the stainless-steel cylinder containing H_2O, was kept at room temperature. Each ALD cycle is comprised of a 0.5 s TTIP pulse, 20 s residence time, 10 s Ar purging time, 2 s H_2O pulse, 15 s residence time, 10 s Ar purging time (at 50 sccm), leading to an operating pressure of 1.8 torr during the precursor pulse timing. The feeding of the precursors into the ALD reactor chamber was carried out by two individual inlets to avoid cross contaminations. The titanium oxide ALD process on carbon nanotubes has already been reported by our group.[17] 200 ALD cycles were carried out to ensure a conformal and continuous coating of the nanotubes.

2.2. ALD/MLD of Fe-NH_2TP

The organic–inorganic hybrid thin films were grown by combining ALD and MLD cycles, on a custom-made cross-flow ALD reactor working in continuous mode, from $Fe(thd)_3$ and NH_2TPA. The Si/SiO_2 (1.5 cm × 1.5 cm) substrates were cleaned in a freshly prepared piranha solution (1 : 3 H_2O_2/H_2SO_4 mixture) for 30 minutes. Followed by washing with distilled water and then blown-dry by compressed air. These substrates were firstly used for the hybrid film growth. The individual precursors were sequentially pulsed into the reaction chamber,

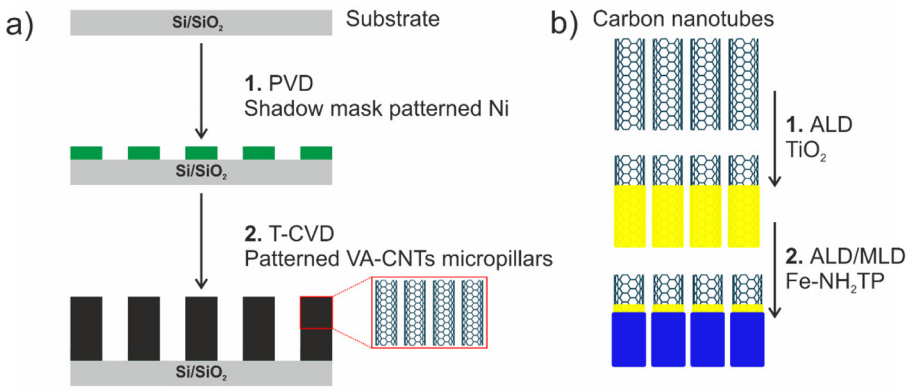

Fig. 1 (a) Schematic representation of the vertically aligned carbon nanotubes (VA-CNTs) patterning sequence based on shadow mask Ni deposition. (b) Carbon nanotubes coating steps (1, 2) to form a core–shell–shell heterostructure; carbon nanotubes (inner core)/titanium oxide (first shell)/Fe-NH_2TP (second shell).

from stainless-steel cylinders, which were kept at 130 °C (Fe(thd)$_3$) and 230 °C (NH_2TA) to achieve enough vapor pressure for pulsing. The stainless-steel tubing lines were heated at 140 °C to prevent vapor condensation. The temperatures were stabilized before starting the depositions. In a typical process, each ALD/MLD cycle consisted of a 1.0 s Fe(thd)$_3$ pulse, 2.0 s NH_2TPA pulse, with 2.0 s and 4.0 s in between to separate the precursor's pulses at 180 °C. N_2 was the carrier and purging gas and a total flow of 100 sccm was used, leading to an operating pressure of 1.7 torr. The feeding of the precursors into the ALD reactor chamber was carried out by two individual inlets to avoid cross contaminations. All experimental parameters were selected accordingly to a preliminary set of experiments and literature reports, in particular Karppinen's group work dealing with Fe-based ALD/MLD processes (Table S1†). 1000 cycles were used during Fe-NH_2TP to achieve a thickness of *ca.* 126 nm (180 °C). Several samples were prepared at different deposition temperatures, as the thin film properties strongly depend on this parameter, while the number of cycles was kept constant.

2.3. Characterization

The Fe-NH_2TP films were characterized by Scanning Electron Microscopy (SEM) on a Hitachi SU-70 microscope operated in the secondary electron mode at 15 kV and equipped with energy-dispersive X-ray spectroscopy (EDX). The samples were sputter-coated with a thin layer of carbon. The surface topography of the films was imaged by atomic force microscopy (AFM) on a Ntegra Prima setup (NT-MDT) in the tapping mode, under ambient conditions. A silicon cantilever (Nanosensor PPP-NCHR) with the spring constant of $k \approx 42$ N m^{-1} and tip radius <10 nm was used. Surface roughness was determined as root-mean-square value (R_q) by using the WSxM 5.0 software. The crystallographic nature of the thin films was characterized by grazing incidence X-ray diffraction mode on a Philips X'Pert MRD diffractometer with Cu K_α (λ = 1.5418 Å) radiation. The X-rays were generated by applying 45 kV voltage on Cu anode at a current of 40 mA. The thickness of Fe-NH_2TP films deposited on the Si/SiO_2 wafer substrates was measured by X-ray reflectance on the same diffractometer. Raman spectroscopy (Jobin Yvon T64000) was carried out at a 532 nm excitation wavelength on the as-grown nanotubes at room temperature. The I_D/I_G ratio value was estimated from integrated area intensities of the D and G band peaks. Attenuated total reflectance Fourier transform infrared measurements were performed on a Bruker Tensor 27 at 4 cm^{-1} resolution to assess the bonding structure. A spectrum of an uncoated Si/SiO_2 was subtracted from the spectra to compensate for the effect of the substrate. Wettability measurements were performed on a commercial contact angle system (Dataphysics OCA) using deionized water (Milli-Q, drop volume 3 μL). The static contact angle was measured on five different locations for each sample, in an air at room temperature. The morphology and the microstructure of the Fe-NH_2TP films on the nanotubes were investigated by Scanning Transmission Electron Microscopy (STEM; Hitachi HD2700, operated at 200 kV) equipped with energy-dispersive X-ray spectroscopy (EDX) for elemental analysis and by Transmission Electron Microscopy (JEOL JEM-2200FS, operated at 200 kV). Digital micrograph software (Gatan, Inc.) was used to analyze the images. The samples for STEM and TEM measurements were prepared by dry adhesion of the coated nanotubes to a holey carbon film supported on a copper grid, after removing them from the substrate surface.

3. Results and discussion

3.1. Fe-NH_2TP on Si/SiO_2 support

Iron(III)-2-amino terephthalate (Fe-NH_2TP) hybrid thin films were deposited by ALD/MLD from Fe(thd)$_3$ as iron source and NH_2TPA the organic precursor at 170 °C, 180 °C and 250 °C, because the thin film's structure and properties strongly depend on temperature. In our previous work[18] we grew *in situ* crystalline Eu-NH_2TP inorganic–organic hybrid thin films at 180 °C. Encouraged by this result, we have used this deposition temperature as a guideline to growth the films on Si/SiO_2 substrates, before ALD/MLD coating of patterned vertically aligned carbon nanotube micropillars.

Fig. S2a of ESI† shows the X-ray reflectance data and SEM image of the Fe-NH_2TP film after 1000 ALD/MLD cycles, at 180 °C. The total film thickness determined by the former was 126.1 nm in good accord with the SEM average value of 125.0 nm (Fig. S2b†). As confirmed by grazing incident X-ray diffraction, the Fe-NH_2TP film is amorphous (Fig. S2c†) and exhibits low surface roughness, witnessed by atomic force microscopy, with root-mean-square (R_q) roughness of 0.61 nm (170 °C), 0.64 nm (180 °C) and 0.93 nm (250 °C) determined from a 500 nm × 500 nm images (Fig. S3†) and the film's surface is smooth. In addition, R_q values are much smaller than the Fe-NH_2TP thickness. Thus, the whole Si/SiO_2 surface is readily covered with Fe-NH_2TP, in all samples. The X-ray reflection plot revealed a film density (ρ_m) of 1.58 g cm^{-3}, on the basis of the so-called critical angle (θ_c).[19]

The infrared spectra of the Fe-NH_2TP thin film depict the characteristic symmetric $\nu_S(COO^-)$ and asymmetric $\nu_{AS}(COO^-)$ stretching bands at 1383.4 cm^{-1} and 1569.2 cm^{-1}, respectively, and the absence of peaks at *ca.* 1700 cm^{-1} (ν(C=O)) ascribed to free carboxylic acid groups, showing the deprotonation of the carboxylate groups and coordination to iron (Fig. 2). The obtained values match those observed for a NH_2-MIL101 (Fe) powdered sample synthesized in solution[20] as a reference for this study (powder XRD pattern is depicted in Fig. S4†). The difference $\Delta\nu = \nu_{AS} - \nu_S$ provides information on the carboxylate-to-Fe^{3+} coordination mode. The observed $\Delta\nu$ = 185.8 cm^{-1} falls in the range 130–200 cm^{-1} indicating a bridging-type bonding between the carboxylate group and two Fe^{3+} ions.[21] The bands at 1253.1 cm^{-1} and 770.6 cm^{-1} are assigned to ν(C–N) and ν(C–H) benzene ring vibrations, respectively. The presence of –NH_2 group is witnessed by the lower intensity peaks at 3446.1 cm^{-1} and 3347.3 cm^{-1}, that are still present in the spectrum of the film, though broadened. These findings are also consistent with the literature on the molecular struc-

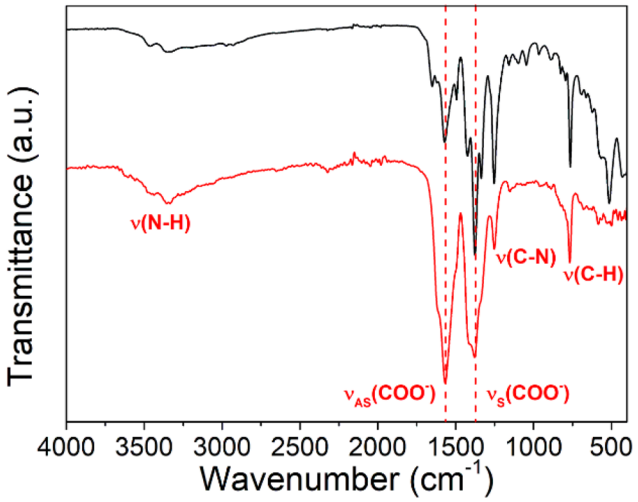

Fig. 2 Attenuated total reflectance Fourier transform infrared spectra of NH_2-MIL101 (Fe) powdered sample (black line), and as-deposited Fe-NH_2TP on Si/SiO_2 support thin films (red line) prepared at 170 °C, after 1000 ALD/MLD cycles.

ture of NH_2-Fe-MIL materials.[20,22] The infrared spectra also confirm the formation of Fe-NH_2TP hybrid films at deposition temperatures ranging between 170 °C and 250 °C (Fig. S5†), while the deposition temperatures employed in the Fe-based ALD/MLD processes depicted in Table S1† are between 240 °C and 360 °C. The normalized results indicate that there are no significant changes in the peak intensities with the deposition temperature, suggesting uniform films thickness.[23]

3.2. Fe-NH_2TP on TiO_2/VA-CNTs

The BF-TEM image of the uncoated nanotubes showed that all of them were multiwalled (Fig. S6a†). Raman spectroscopy is a widely used method to characterize carbon nanotube structures due to its versatility.[24,25] In graphitic materials, C–C bond stretching generates the so-called G-band, which is present in all sp^2 carbon systems. The D-band, on the other hand, is linked to the presence of defects on the hexagonal sp^2 network. Fig. S6b† presents a representative Raman spectrum, displaying the two main bands, D-band and G-band, characteristic of multiwalled nanotubes. This finding is consistent with BF-TEM analysis. The integrated area intensity ratio of D-band to G-band (I_D/I_G) provides valuable insights into the level of disorder or defects on the nanotubes' surface. The estimated I_D/I_G ratio is approximately 1.5, indicating a higher degree of disorder or defects on the surface, which plays a crucial role in the nucleation of ALD metal oxides.[26] It is worth noting that a low defect density is indicated by a small I_D/I_G ratio value.[24] Consider the core–shell–shell heterostructure preparation process illustrated in Fig. 1b. Firstly, the low temperature water-based titanium oxide ALD conditions and parameters were optimized to ensure a conformal and homogeneous deposition that maximizes the density of reactive sites on the nanotubes surface promoting the nucleation of the hybrid thin film. Moreover, titanium oxide adhesion layer provides a high concentration of oxygen-containing surface groups, such as –OH, that interact with the $Fe(thd)_3$ precursor, thus promoting the nucleation of Fe-NH_2TP on the nanotube's surface, and eventually the thin film growth. In turn, the carbon nanotubes have a suitable density of surface defects, consistent with the Raman studies, allowing the nucleation of titanium oxide affording suitable conformal thin films, as shown in Fig. S7.†

Raman spectroscopy was also carried out on the titanium oxide-coated nanotubes (Fig. S8†). However, no significant changes were observed in the typical D-band and G-band shape. Therefore, it can be inferred that the ALD titanium oxide deposition had little to no effect on the nanotubes, and no features were detected in the region where anatase modes were expected (marked with the red dashed square). This indicates that the titanium oxide did not exhibit any crystallinity features, which is consistent with the low deposition temperature of approximately 100 °C.[16] Furthermore, grazing incident X-ray diffraction analysis of the titanium oxide films on the Si/SiO_2 substrate confirmed that they were amorphous (Fig. S9†). Upon ALD/MLD treatment, SEM and STEM show that the morphology of the vertically aligned carbon nanotube micropillars is retained, while EDX indicates the presence of both titanium oxide and Fe-NH_2TP on the nanotube's surface (Fig. 3, 4 and S10†). To perform STEM and TEM imaging, some coated nanotubes were removed from the Si/SiO_2 surface and transferred by dry adhesion to a holey carbon film supported on a copper grid.

The Secondary Electrons (SE)-STEM mode image shown in Fig. 4a provides rich depth information on the film's surface topography. On the other hand, Transmission Electron (TE)-STEM mode images of the Fe-NH_2TP thin film confirm the coating is conformal and homogeneous, with an average 9.4 ± 0.3 nm thickness, and grows under surface-controlled deposition (Fig. 4b). The corresponding Z-Contrast (ZC)-STEM mode image is highly sensitive to the atomic number of the elements[27] and exhibits brightness variations across the thin film, with iron clearly showing up in the outer shell (Fig. 4c). The granular-like surface morphology of the deposited film is clearly shown by the different imaging modes. The absence of other elements assures the purity of the sample. No apparent segregation occurs along the nanotube's length.

Fig. 5a shows the Bright Field (BF-)TEM image of the carbon nanotubes/titanium oxide/Fe-NH_2TP heterostructures. The High-Resolution (HR-)TEM micrograph, fast Fourier transform, and inverse fast Fourier transform images (Fig. 5b, d and e) clearly show that the Fe-NH_2TP hybrid film coating is amorphous, *i.e.*, with no long-range order, in accord with the grazing incidence X-ray diffraction measurements (Fig. 5c). The observed faint reflection at 26° 2θ is assigned to (002) plane of the carbon nanotubes corresponding to the characteristic 0.34 nm inter-wall spacing of the carbon nanotubes depicted in Fig. 5b.

The hydrophobic properties of the carbon nanotubes/titanium oxide/Fe-NH_2TP were evaluated by determining their water contact angles (as shown in Fig. 6 and Fig. S11†). Having a hydrophobic surface is crucial when the performance and

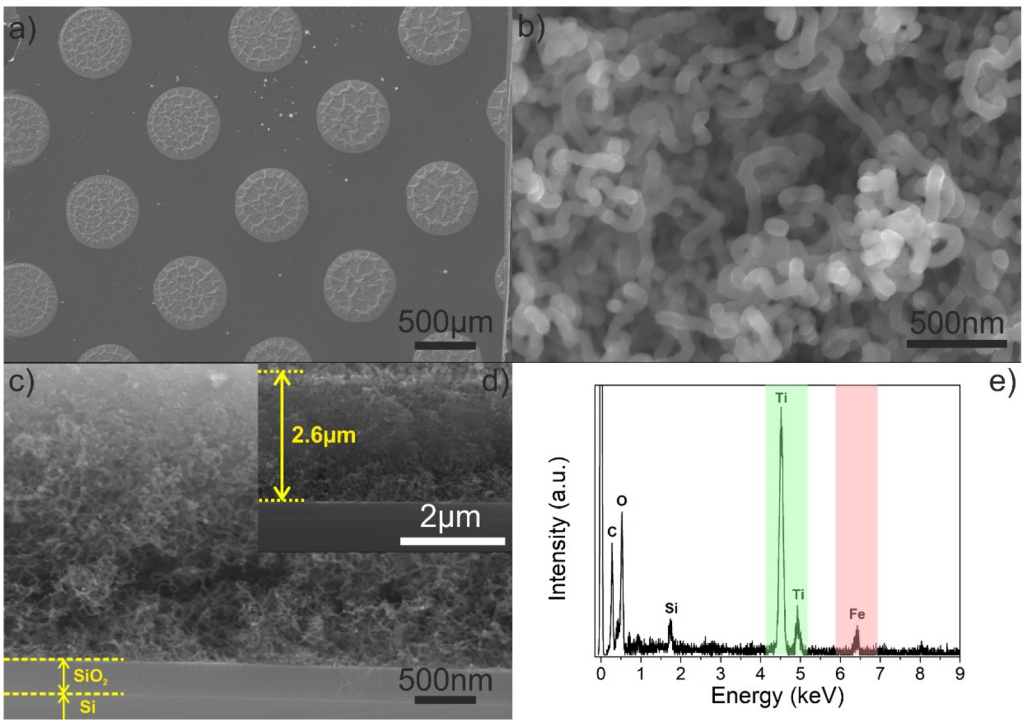

Fig. 3 (a and b) Top-view SEM image of the vertically aligned carbon nanotube micropillars, taken at (a) low and (b) high magnification; (c and d) cross-section image showing the alignment of the nanotubes with a significant entanglement among nanotubes, after titanium oxide ALD (200 cycles) followed by Fe-NH_2TP ALD/MLD (1000 cycles) at 180 °C. (e) The EDX spectrum confirms the presence of Ti and Fe on the nanotubes surface.

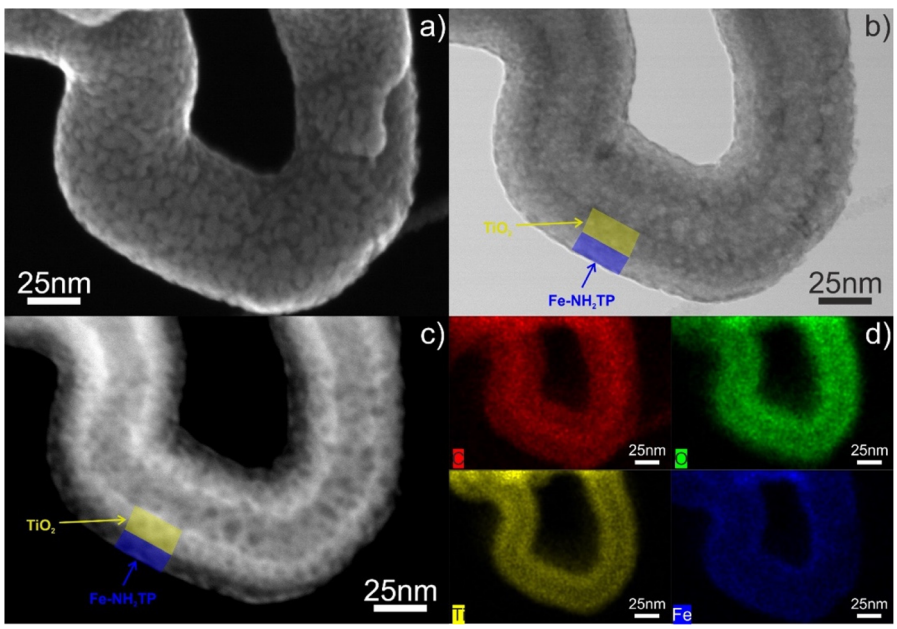

Fig. 4 (a) SE-STEM, (b) TE-STEM, and (c) ZC-STEM mode images, and (d) EDX elemental mapping of an individual nanotube coated with titanium oxide and Fe-NH_2TP.

durability of the devices may be impacted by the presence of moisture.[28,29] The water contact angles of the composite thin films were measured at 170 °C and 250 °C, and were found to be 107.5 ± 1.7° and 107.5 ± 1.8°, respectively, which is in stark contrast to the uncoated Si/SiO_2 substrate, which had a contact angle of 52.2 ± 1.2°. This data demonstrates that the hybrid

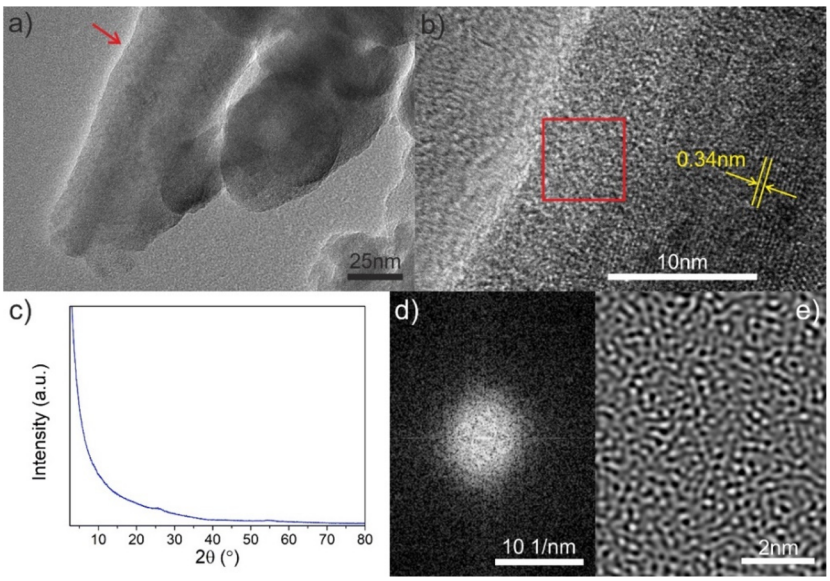

Fig. 5 (a) BF-TEM image of nanotubes coated with titanium oxide and Fe-NH_2TP. (b) HR-TEM image taken from the area depicted by the red arrow in (a); (c) GIXRD pattern of vertically aligned carbon nanotubes coated with titanium oxide and Fe-NH_2TP; (d) fast Fourier transform, and (e) inverse fast Fourier transform of the area depicted by the red square shown in (b).

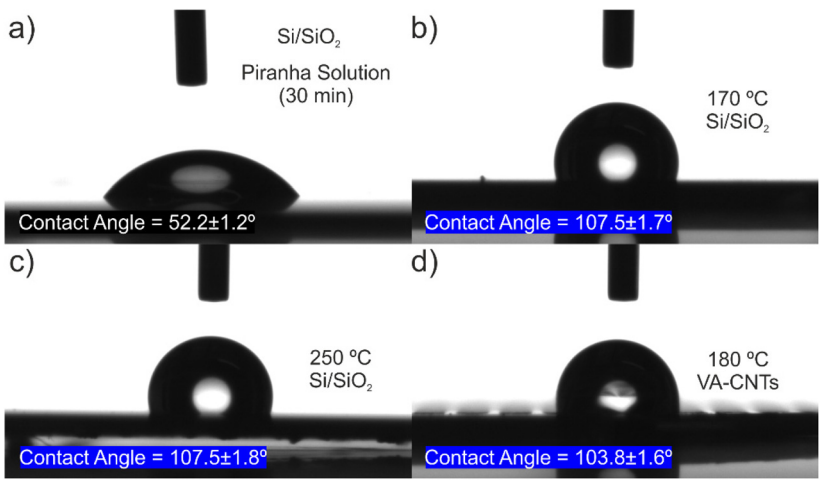

Fig. 6 Water contact angles on: (a) bare Si/SiO_2 substrate; Fe-NH_2TP thin films on Si/SiO_2 at (b) 170 °C and at (c) 250 °C; (d) carbon nanotubes/titanium oxide/Fe-NH_2TP at 180 °C (3 μL of water droplets on different substrates).

composites exhibit a highly hydrophobic nature, while the uncoated substrate is hydrophilic (having a contact angle less than 90°).[28,29] As a result, water droplets generally do not adhere well to these surfaces and tend to roll off easily.

This work presents the potential of employing hydrophobic Fe-NH_2TP for the removal of organic dyes from aqueous solutions.[30] However, the practical performance of Fe-NH_2TP could be hindered by the competitive adsorption of water. Nevertheless, the heterostructure configuration could serve as an excellent platform for organic dye removal. Here, the active Fe-NH_2TP is immobilized over a sizable support structure comprised of vertically aligned carbon nanotubes. This configuration favors an enhancement in both the adsorption efficiency and capacity, making it a promising solution for dye remediation.

4. Conclusions

Iron-2-amino terephthalate (Fe-NH_2TP) hybrid thin films were deposited on Si/SiO_2 and vertically aligned carbon nanotube micropillar substrates using the ALD/MLD process at 180 °C, yielding amorphous films with a smooth surface morphology, as confirmed by grazing incidence X-ray diffraction and atomic force microscopy studies, respectively. The formation of Fe-NH_2TP was further verified by Fourier transform infrared spec-

troscopy, which showed the carboxylate-to-Fe^{3+} coordination mode. This work also highlighted the successful fabrication of a core–shell–shell heterostructure comprising carbon nanotubes/TiO_2/Fe-NH_2TP. Scanning transmission electron microscopy and accompanying energy-dispersive spectroscopy elemental mapping revealed an even distribution of C, O, Ti, and Fe on the surface of the carbon nanotubes. The amorphous nature of the Fe-NH_2TP hybrid film was also confirmed by high-resolution transmission electron microscopy. The hydrophobic character of the hybrid films was demonstrated through water contact angle measurements, making them suitable for use in moist environments. This study sheds new light on the thin film processing of inorganic–organic hybrid heterostructures by ALD/MLD. It highlights the potential utility of these structures in, for example, applications related to surface wettability, such as hydrophobic dye adsorption, where conventional solution-based preparation methodologies are not viable.

Author contributions

R. M. Silva: conceptualization, methodology, investigation, validation, formal analysis, writing – original draft, and writing – review and editing; J. Rocha: conceptualization, methodology, validation, supervision, resources, funding acquisition, writing – review and editing; Rui F. Silva: conceptualization, methodology, validation, supervision, resources, funding acquisition, writing – review and editing.

Conflicts of interest

There are no conflicts to declare.

Acknowledgements

This work was developed within the scope of the project CICECO-Aveiro Institute of Materials, UIDB/50011/2020, UIDP/50011/2020 & LA/P/0006/2020, financed by national funds through the FCT/MCTES (PIDDAC). The authors acknowledge Dr R. Soares, MSc. M. Ferro and Dr S. Peripolli for assistance with the XRR/GIXRD and STEM/HRTEM measurements, respectively. Dr F. Figueira is acknowledged for the synthesized NH_2-MIL 101 (Fe) powder sample, used as a reference.

References

1 J. Multia and M. Karppinen, *Adv. Mater. Interfaces*, 2022, **9**, 2200210.
2 J. Ren and T.-C. Jen, *Coord. Chem. Rev.*, 2021, **430**, 213734.
3 R. L. Puurunen, *Chem. Vap. Deposition*, 2014, **20**, 332–344.
4 Y. Fang, Z. Yang, H. Li and X. Liu, *Environ. Sci. Pollut. Res.*, 2020, **27**, 4703–4724.
5 C. R. Quijia, C. Lima, C. Silva, R. C. Alves, R. Frem and M. Chorilli, *J. Drug Delivery Sci. Technol.*, 2021, **61**, 102217.
6 M. Y. Zorainy, M. G. Alalm, S. Kaliaguine and D. C. Boffito, *J. Mater. Chem. A*, 2021, **9**, 22159–22217.
7 I. Stassen, D. De Vos and R. Ameloot, *Chem. – Eur. J.*, 2016, **22**, 14452–14460.
8 C. Crivello, S. Sevim, O. Graniel, C. Franco, S. Pané, J. Puigmartí-Luis and D. Munõz-Rojas, *Mater. Horiz.*, 2021, **8**, 168–178.
9 H. O. Pierson, *Handbook of Chemical Vapor Deposition*, William Andrew, Elsevier, 1997.
10 I. Stassen, M. Styles, G. Grenci, H. Van Gorp, W. Vanderlinden, S. De Feyter, P. Falcaro, D. De Vos, P. Vereecken and R. Ameloot, *Nat. Mater.*, 2016, **15**, 304–310.
11 M. Knez, K. Nielsch and L. Niinistö, *Adv. Mater.*, 2007, **19**, 3425–3438.
12 C. Guan and J. Wang, *Adv. Sci.*, 2016, **3**, 1500405.
13 H. V. Bui, F. Grillo and J. R. Ommen, *Chem. Commun.*, 2017, **53**, 45–71.
14 M. Lie, H. Fjellvåg and A. Kjekshus, *Thin Solid Films*, 2005, **488**, 74–81.
15 A. Corletto and J. G. Shapter, *Adv. Sci.*, 2021, **8**, 2001778.
16 I. E. Oliveira, R. M. Silva, A. V. Girão, J. Faria, C. G. Silva and R. F. Silva, *Eur. J. Inorg. Chem.*, 2020, **18**, 1743–1750.
17 I. E. Oliveira, R. M. Silva, J. Rodrigues, M. R. Correia, T. Monteiro, J. Faria, R. F. Silva and C. G. Silva, *RSC Adv.*, 2022, **12**, 16419–16430.
18 R. M. Silva, L. D. Carlos, J. Rocha and R. F. Silva, *Appl. Surf. Sci.*, 2020, **527**, 146603.
19 J. Penttinen, M. Nisula and M. Karppinen, *Chem. – Eur. J.*, 2019, **25**, 11466–11473.
20 X. Y. Dao, J.-H. Guo, Y.-P. Wei, F. Guo, Y. Liu and W.-Y. Sun, *Inorg. Chem.*, 2019, **58**, 8517–8524.
21 A. Tanskanen and M. Karppinen, *Sci. Rep.*, 2018, **8**, 8976.
22 Q. Xie, Y. Li, Z. Lv, H. Zhou, X. Yang, J. Chen and H. Guo, *Sci. Rep.*, 2017, **7**, 3316.
23 A. Philip, S. Vasala, P. Glatzel and M. Karppinen, *Dalton Trans.*, 2021, **50**, 16133–16138.
24 A. C. Ferrari and J. Robertson, *Phys. Rev. B: Condens. Matter Mater. Phys.*, 2000, **20**, 14095.
25 M. S. Dresselhaus, G. Dresselhaus, R. Saito and A. Jorio, *Phys. Rep.*, 2005, **409**, 47–99.
26 R. M. Silva, M. C. Ferro, J. R. Araujo, C. A. Achete, G. Clavel, R. F. Silva and N. Pinna, *Langmuir*, 2016, **32**, 7038–7044.
27 C. Wiktor, M. Meledina, S. Turner, O. I. Lebedevd and R. A. Fischer, *J. Mater. Chem. A*, 2017, **5**, 14969–14989.
28 K. Jayaramulu, F. Geyer, A. Schneemann, S. Kment, M. Otyepka, R. Zboril, D. Vollmer and R. A. Fischer, *Adv. Mater.*, 2019, **31**, 1900820.
29 L. H. Xie, M. M. Xu, X. M. Liu, M. J. Zhao and J. R. Li, *Adv. Sci.*, 2020, **7**, 1901758.
30 Q. Zha, X. Sang, D. Liu, D. Wang, G. Shi and C. Ni, *J. Solid State Chem.*, 2019, **275**, 23–29.